Spatial Modelling of Retinal Thickness in Images from Patients with Diabetic Macular Oedema

Wenyue Zhu[1(✉)], Jae Yee Ku[1,2], Yalin Zheng[1,2], Paul Knox[1,2], Simon Harding[1,2], Ruwanthi Kolamunnage-Dona[3], and Gabriela Czanner[1,4]

[1] Department of Eye and Vision Science, Institute of Ageing and Chronic Disease, University of Liverpool, Liverpool L7 9TX, UK
{Wenyue.Zhu,yzheng}@liverpool.ac.uk
[2] St Paul's Eye Unit, Royal Liverpool University Hospital, Liverpool L7 8XP, UK
[3] Department of Biostatistics, University of Liverpool, Liverpool L69 3GL, UK
[4] Department of Applied Mathematics, Liverpool John Moores University, Liverpool L3 3AF, UK
G.Czanner@ljmu.ac.uk

Abstract. For the diagnosis and monitoring of retinal diseases, the spatial context of retinal thickness is highly relevant but often underutilised. Despite the data being spatially collected, current approaches are not spatial: they involve analysing each location separately, or they analyse all image sectors together but they ignore the possible spatial correlations such as linear models, and multivariate analysis of variance (MANOVA). We propose spatial statistical inference framework for retinal images, which is based on a linear mixed effect model and which models the spatial topography via fixed effect and spatial error structures. We compare our method with MANOVA in analysis of spatial retinal thickness data from a prospective observational study, the Early Detection of Diabetic Macular Oedema (EDDMO) study involving 89 eyes with maculopathy and 168 eyes without maculopathy from 149 diabetic participants. Heidelberg Optical Coherence Tomography (OCT) is used to measure retinal thickness. MANOVA analysis suggests that the overall retinal thickness of eyes with maculopathy are not significantly different from the eyes with no maculopathy ($p = 0.11$), while our spatial framework can detect the difference between the two disease groups ($p = 0.02$). We also evaluated our spatial statistical model framework on simulated data whereby we illustrate how spatial correlations can affect the inferences about fixed effects. Our model addresses the need of correct adjustment for spatial correlations in ophthalmic images and to improve the precision of association in clinical studies. This model can be potentially extended into disease monitoring and prognosis in other diseases or imaging technologies.

Keywords: Spatial modelling · Correlated data · Simulation · Retinal imaging · Diabetic Macular Oedema

Y. Zheng et al. (Eds.): MIUA 2019, CCIS 1065, pp. 1–13, 2020.
https://doi.org/10.1007/978-3-030-39343-4_10

1 Introduction

Diabetic Macular Oedema (DMO) is a consequence of diabetes that involves retinal thickness changes in the area of the retina called the macula. Although the macula is only approximately 5 mm in diameter, the densely pack photoreceptors in the macula give rise to our central high acuity and colour vision. A healthy macula plays an essential role for activities such as reading, recognizing faces and driving. Macular disease can cause loss of central vision; DMO is the most common cause of vision loss among people with diabetic retinopathy.

DMO is caused by an accumulation of fluid (oedema) in the macula thought to be secondary to vascular leakage. It has been proposed that macular thickness is associated with visual loss [9]. For measuring retinal thickness, OCT is now widely used for the diagnosis and monitoring of DMO as it is able to produce high-resolution cross-sectional images of the retina [12].

The macula is often divided into nine subfields as initially described by the Early Treatment of Diabetic Retinopathy Study (ETDRS) research group [11]. These subfields comprise three concentric circles/rings with radii of 500, 1500 and 3000 μm subdivided into four regions (superior, temporal, inferior and nasal) as shown in Fig. 1. These subfields are named by their location as the central (CS), superior inner (SI), temporal inner (TI), nasal inner (NI), superior outer (SO), temporal outer (TO), inferior outer (IO) and nasal outer (NO). OCT measurements provide retinal thickness measurements for each of these nine subfields.

The simplest approach to analyse retinal thickness in these nine subfields is to analyse them separately in nine separate analyses. Sometimes only the measurement of the central subfield is used and the other measurements are discarded. However, this ignore the spatial context of measurements. If spatial dependency between the measurements of different subfields is not analysed properly, it can affect the precision of estimates and lead to inaccurate results in statistical tests.

A more complex approach is to properly spatially analyse the data [6]. Spatial statistical model takes into account the spatial correlations [4] thus in our data provides a means of incorporating spatial information from retinal thickness measurements in different subfields into statistical analyses. It may provide information of value in discriminating between disease states and for detection of retinal disease [7]. It has already been applied widely in other medical imaging contexts such as functional neuroimaging and cardiac imaging, where spatial correlations are also captured in the model. For example, Bowman et al. constructed a spatial statistical model for cardiac imaging from single photon emission computed tomography (SPECT) [2], and Bernal-Rusiel et al. explored the spatial structures in Magnetic Resonance Image (MRI) data in patients with Alzheimer's disease [1]. However, the application of spatial statistics to ophthalmic images has not yet been extensively studied.

Another concern in the analysis of ophthalmic images is the unit of analysis issue. Often, the correlation between two eyes from the same individual is ignored. Treating the eyes as independent introduces spuriously small standard errors. Although there is a continuing concern regarding this problem and methods [15,16]

are available for adjusting the correlation between the two eyes, the majority of studies do not take this into account when data from both eyes are available. This methodological problem has not improved much over the past two decades [17].

In this paper, we aimed to present a new statistical spatial inference framework for retinal images and to study the effect of the spatial correlations on the analysis of the spatial data. This framework is based on a linear mixed effect model with a spatial (Gaussian, autoregressive-1, exponential and spherical) error structure for the analysis of OCT imaging data, where correlation between eyes from the same patient and demographic data is adjusted in the model. We conducted a simulation study to validate our model and study the benefits of using a spatial modelling framework when spatial correlations exist.

The organization of the rest of the paper is as follows. The image dataset and the statistical modelling framework are presented in Sect. 2. In Sect. 3, we present results from the real data set. Simulation setting and simulation results are presented in Sect. 4. Discussion of our work and the conclusion are presented in Sects. 5 and 6.

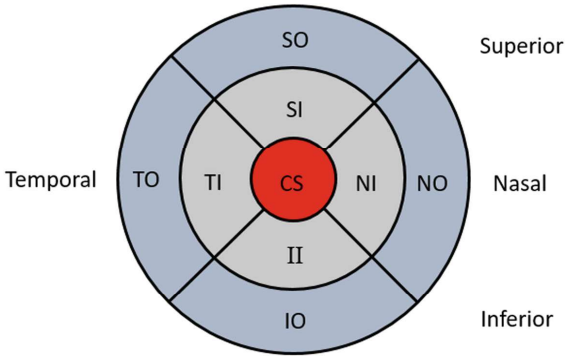

Fig. 1. Early Treatment of Diabetic Retinopathy (ETDRS) gird centred on the fovea with the radii of the central circle being 500 µm, inner circle 1500 µm and outer circle 3000 µm and the nine sectors (also called subfields).

2 Methods

2.1 Image Dataset

To illustrate the use of our proposed model, we apply it to retinal thickness measurements from the Early Detection of Diabetic Macular Oedema (EDDMO) study which is a prospective observational study conducted in the Royal Liverpool University Hospital. This study was performed in accordance with the ethical standards laid down in the Declaration of Helsinki, with local ethical and governance approval.

There were 150 participants with diabetes at their baseline visit in the study. Self-reported ethnic background revealed that approximately 90% of the participants were Caucasians. Participants with diabetes and co-existing pathologies (intracranial lesions n = 1, and ocular pathologies n = 4) were excluded from the analysis. A small number of participants did not have data collected from both eyes. All participants were examined by an ophthalmologist with a slit lamp. All the participants with diabetes had a dilated fundoscopy examination. Based on examination findings, eyes of participants with diabetes were categorized into two groups, either no maculopathy (M0) or maculopathy (M1). A summary of the dataset stratified by clinical diagnosis based on slit lamp examination is shown in Table 1. Retinal thickness measurements for both eyes were obtained using Heidelberg Spectralis OCT. Although the measurements of both foveal centre point thickness and central subfield mean thickness are available using OCT, central subfield mean thickness is more commonly used in clinical research when tracking center-involving DMO [3]. Therefore only central subfield mean thickness (CS) is used in the statistical analysis in this paper.

Table 1. Number of eyes for the analysis of overall thickness of retina

	M0	M1	Total
Left eyes	91	40	131
Right eyes	77	49	126
Total	168	89	257

2.2 Statistical Model

Our spatial statistical model has the general form described in Eq. (1), which is based on a linear mixed effect model with two-level of nested random effects.

In the model, $\boldsymbol{Y}_{ij}$ is the response vector for ith individual in the nested level of grouping, $\boldsymbol{X}_{ij}$ is the fixed effect vector (e.g. age, age, sex, glycated haemoglobin (HbA1c), axial length) associated with *beta*, b_i is the first level of random effects (e.g. individual level random effect) associated with $\boldsymbol{Z}_i$, and u_{ij} is the second level of random effects (e.g. eye level random effect nested within each individual) associated with $\boldsymbol{D}_{ij}$.

$$\begin{gathered} \boldsymbol{Y}_{ij} = \boldsymbol{X}_{ij}\beta + \boldsymbol{Z}_i b_i + \boldsymbol{D}_{ij} u_{ij} + \boldsymbol{\epsilon}_{ij}, \qquad i = 1, ..., m; j = 1, ..., n_i \\ b_i \sim N(0, \boldsymbol{G}_1), \qquad u_{ij} \sim N(0, \boldsymbol{G}_2), \qquad \epsilon_{ij} \sim N(0, \boldsymbol{\Sigma}_s) \end{gathered} \tag{1}$$

where the first level random effect b_i is independent of the second level random effect u_{ij}, and $\boldsymbol{\epsilon}_{ij}$ are within group error representing spatial correlation in the images which is assumed to be independent of random effect.

2.3 Spatial Dependency

The covariance matrix $\boldsymbol{\Sigma}_s$ for ϵ_{ij} can be decomposed to $\boldsymbol{\Sigma}_s = \sigma_s^2 \boldsymbol{\Psi}_{ij}$ where $\boldsymbol{\Psi}_{ij}$ is a positive-definite matrix which can be decomposed to $\boldsymbol{\Psi}_{ij} = \boldsymbol{\Lambda}_{ij} \boldsymbol{C}_{ij} \boldsymbol{\Lambda}_{ij}$. $\boldsymbol{\Lambda}_{ij}$ is a diagonal matrix and $\boldsymbol{C}_{ij}$ is correlation matrix with parameter γ. In our model, $\boldsymbol{\Lambda}_i$ is a identity matrix and it is easy to write that $cor(\epsilon_{ijk}, \epsilon_{ijk'}) = [\boldsymbol{C}_{ij}]_{kk'}$.

The spatial dependency $cor(\epsilon_{ijk}, \epsilon_{ijk'})$ is modelled with four different structures where the correlation is modelled as autoregressive-1 model, Gaussian model, exponential model and spherical model where γ can take the value of γ_a, γ_g, γ_e, γ_s respectively.

For the lag autoregressive model, the correlation function decreases in absolute value exponentially with lag δ ($\delta = 1, 2, ...$) model has the form of

$$s_{kk'} = \gamma_a^{\delta}, \tag{2}$$

For spatial structured correlation, if $d_{kk'}$ is denoted as the Euclidean distance between location k and $k^{'}$. The Gaussian correlation has the form of,

$$s_{kk'} = exp(-\gamma_g d_{kk'}^2), \tag{3}$$

the exponential model has the form of

$$s_{kk'} = exp(-\gamma_g d_{kk'}), \tag{4}$$

and the spherical model has the form of

$$s_{kk'} = 1 - 1/2(3\gamma_s d_{kk'} - \gamma_s^3 d_{kk'}^3). \tag{5}$$

2.4 Statistical Inference

In a traditional mixed effect model defined by Laird and Ware [5], the maximum likelihood estimator $\hat{\beta}$ for fixed effect β is as follows,

$$\hat{\beta} = (X^{'} \Sigma X)^{-1} X^{'} \Sigma^{-1} (Y - Z\hat{b}) \tag{6}$$

with the prediction $\hat{b}$ for random effect is obtained as follows,

$$\hat{b} = (Z^{'} \Sigma_0^{-1} Z + G_0^{-1})^{-1} Z^{'} \Sigma_0^{-1} (Y - X\beta_0) \tag{7}$$

where $Y|b \sim N(X\beta + Zb, \Sigma)$, $b \sim N(0, G)$ and Σ_0, G_0 β_0 are given values in EM algorithm during iterations. And the maximum likelihood estimator $\hat{\theta}$ for the precision estimates which define the parameters in the overall covariance matrix can be optimized through EM iterations or Newton-Raphson iterations [5].

If we describe a two level random effect model ignoring the spatial dependency, which assume $\boldsymbol{\Psi_{ij}}$ in model (1) as a identity matrix. We will have

$$\begin{gathered} \boldsymbol{Y}_{ij}^* = \boldsymbol{X}_{ij}^* \beta + \boldsymbol{Z}_i^* b_i + \boldsymbol{D}_{ij}^* u_{ij} + \boldsymbol{\epsilon}_{ij}^*, \qquad i = 1, ..., m; j = 1, ..., n_i \\ \epsilon_{ij}^* \sim N(0, \sigma_s^2 I) \end{gathered} \tag{8}$$

We define θ_1 as parameter in matrix $\boldsymbol{G}_1$ and θ_2 as parameter in matrix $\boldsymbol{G}_2$. The likelihood function for model (2) can be written as

$$\begin{aligned}&\boldsymbol{L}(\beta,\theta,\sigma_s^2|y^*)=\\&\prod_{i=1}^{m}\int\prod_{j=1}^{n_i}\left[\int p(y_{ij}^*|b_i,u_{ij},\beta,\theta_s^2)p(u_{ij}|\theta_2,\sigma_s^2)du_{ij}\right]p(b_i|\theta_1,\sigma_s^2)\end{aligned}\tag{9}$$

where $p(\cdot)$ is the probability density function. Using the same idea in [5], we have the profiled log-likelihood for $l(\theta_1,\theta_2|y)$. And the maximum likelihood estimator $\hat{\theta}=(\hat{\theta_1},\hat{\theta_2})$ can also be obtained via EM iterations or Newton-Raphson iterations.

If we describe a two level random effect model with the spatial dependency as shown in model (1), we use a linear transformation for y_{ij} with $y_{ij}=(\Psi_{ij}^{-1/2})y_{ij}^*$. Then the likelihood function for model (1) can be written as

$$\begin{aligned}\boldsymbol{L}(\beta,\theta,\sigma_s^2,\gamma|y)&=\prod_{i=1}^{m}\prod_{j=1}^{n_i}p(y_{ij}|\beta,\theta,\sigma_s^2,\gamma)\\&=\prod_{i=1}^{m}\prod_{j=1}^{n_i}p(y_{ij}^*|\beta,\theta,\sigma_s^2)|\Psi_{ij}^{-1/2}|\\&=\boldsymbol{L}(\beta,\theta,\sigma_s^2|y^*)\prod_{i=1}^{m}\prod_{j=1}^{n_i}|\Psi_{ij}^{-1/2}|\end{aligned}\tag{10}$$

Then Eq. (10) can be linked with Eq. (9), leading to a solution for all unknown parameters in model (1).

2.5 Statistical Analysis

In our application for the analysis of the results from the EDDMO study, the model used is described as follows,

$$\begin{aligned}&y_{ijk}=x_{ijk}\beta+b_i+u_{ij}+\epsilon_{ijk},\quad i=1,..,m;j=1,...,n_i;k=1,..,9\\&b_i\sim N(0,\sigma_1^2),\quad u_{ij}\sim N(0,\sigma_1^2),\quad \epsilon_{ij}\sim N(0,\sigma_s^2\boldsymbol{\Psi_{ij}})\end{aligned}\tag{11}$$

where β is a vector, x_{ijk} are covariates for ith participant from j eye in sector k, b_i denotes the random effect for participant i, u_{ij} denote the random effect for j eye in participant i, m is the number of participant and $\max n_i=2$. After statistical analyses, uncorrelated covariates such as sex, duration of diabetes and duration of diabetes were deleted from the model. In the final model, the fixed effect β and the predictor variable x_{ijk} used are follows,

$$\begin{aligned}x_{ijk}\beta=&\beta_0+\beta_1*Age_i+\beta_2*Diagnosis_{ij}\\&+\beta_{3(k)}*Sector_{ijk}+\beta_{4(k)}*Sector_{ijk}*Diagnosis_{ij}\end{aligned}\tag{12}$$

where Age_i is a continuous variable which represent the age for ith participant; $Diagnosis_{ij}$ is a categorical variable represent the diagnosis for j eye from ith participant, which include diabetic eye without maculopathy (baseline) and diabetic eye with maculopathy; $Sector_{ijk}$ is a categorical variable from 1 to 9 which represent the 9 sectors in ETDRS grid with central subfield (CS) thickness as a baseline; $Sector_{ijk} * Diagnosis_{ij}$ represent interaction term between sector and diagnosis with CS*Healthy as baseline.

The mixed effect model with two levels of random effects was fitted using the nlme-R package [10] and the spatial dependency $\boldsymbol{\Psi_{ij}}$ was fitted with structures as described in Sect. 2.3. Missing observations were tested whether they were missing at random and then handled using multiple imputation method in mice-R package [13]. Likelihood ratio test and information criterion (Akaike Information Criterion, AIC; Bayesian information criterion, BIC) were used to compare the models and to find the best model for the inference.

3 Results

To get the visual insight into the data, we made pairwise visualisations of mean profiles of retinal thickness measurements for all nine sectors at patients' baseline visits as shown in Fig. 2. This shows a large within group variability and suggests a pattern for the mean profiles of retinal thickness over the nine sectors. The mean retinal thickness profile of maculopathy group was consistently higher than the no-maculopathy group as shown in Fig. 2.

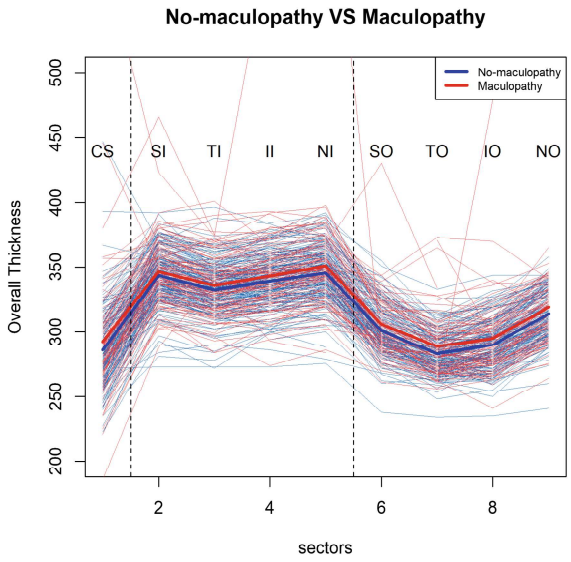

Fig. 2. Pairwise visualizations for mean profiles of retinal overall thickness over 9 sectors at baseline visit

Univariate MANOVA was performed and demonstrated that maculopathy vs no-maculopathy eyes were not different in retinal thickness over the nine sectors ($p = 0.11 > 0.05$). Then we considered the correlations between the two eyes and the spatial correlation between the nine sectors in statistical analyses using our model described in Sect. 2, which also allows heteroscedasticity between groups. We investigated different spatial dependency structures described in Sect. 2.3; an exponential correlation structure was the most informative with the lowest AIC and BIC.

With the two levels of random effects model and an exponential correlation structure, we can detect the difference in the main effect of diagnosis between the maculopathy and no-maculopathy groups ($p = 0.0218 < 0.05$, Table 2). The effect size between groups is 4.4982 with standard error equals 1.9543. Moreover, compared with other correlation structures mentioned in Sect. 2.3, an exponential correlation structure gives the best model with the lowest AIC and BIC. However, we did not detect a shape effect, which is measured as the interaction term between diagnosis and sector mathematically, between maculopathy group and no-maculopathy group ($p = 0.9715$). In the final model as described in Eq. (11), estimators for age, main effect for diagnosis, variance component estimators for random effect and residuals, and heteroscedicity range are shown in Table 2.

Table 2. Estimator for age, main effect, variance component estimators for random effect and residuals, and heteroscedicity range in the final model

			Estimate (Std. Err)	p value
Estimator for age	$\hat{\beta}_1$		−0.2681 (0.0962)	0.0061*
Estimator for main effect	$\hat{\beta}_2$		4.4982 (1.9543)	0.0218*
Variance component	$\hat{\sigma}_1$		15.9307	
	$\hat{\sigma}_2$		7.9328	
	$\hat{\Sigma}_s$	$\hat{\sigma}_s$	22.5541	
		$\hat{\gamma}_e$	0.6620	
Heteroscedicity range among diagnosis group	Maculopathy		1	
	No-maculopathy		0.5790	

*statistically significant with $p < 0.05$

We also found a negative correlation between age and the mean retinal thickness profile ($p = 0.0011$). And we further used a likelihood ratio test to confirm the significance of the eye within patient random effect (u_{ij}) in the model ($p = 0.0005$).

4 Simulation

We carried out a simulation study to check the performance of our final model and to investigate the importance of incorporating spatial correlation in the statistical imaging analyses. We simplified the two-level of nested random effect (11) into a one-level random effect model with spatial exponential correlation. Covariates were chosen based on statistical analyses results from the EDDMO study, including nine locations from the ETDRS grid and a negatively continuous correlated risk factor (e.g. age in EDDMO). Only two disease groups (e.g. maculopathy group versus no-maculopathy group) were considered in the simulation as we are interested the effect of the spatial correlation and the power of our model rather than the clinical outcomes. The aim of our simulation study was to establish how well the spatial approach is able to estimate the risk factor

Table 3. Simulation studies: scenario 1: no correlation between simulated outcomes

Non-spatial approach using linear regression			Spatial approach using linear mixed effect without correlation		
	Risk factor	Diagnosis for main effect		Risk factor	Diagnosis for main effect
True	−0.3	6.1	True	−0.3	6.1
n = 200	β_1	β_2	n = 200	β_1	β_2
Estimates	−0.2997	6.1013	Estimates	−0.2999	6.1015
SE	0.0012	0.1549	SE	0.0013	0.1548
SD	0.0013	0.1449	SD	0.0013	0.1448
CP	95.5%	96.5%	CP	98.5%	95.5%

SE, mean of standard error estimates; SD, Monte Carlo standard deviation of the estimates across the simulated data; CP, coverage probability for the estimates.

Table 4. Simulation studies: scenario 2: moderate exponential spatial correlation between simulated outcomes ($\gamma_e = 0.5$)

Non-spatial approach using linear regression			Spatial approach using linear mixed effect without correlation		
	Risk factor	Diagnosis for main effect		Risk factor	Diagnosis for main effect
True	−0.3	6.1	True	−0.3	6.1
n = 200	β_1	β_2	n = 200	β_1	β_2
Estimates	−0.3001	6.0590	Estimates	−0.3000	6.0585
SE	0.0056	0.6927	SE	0.0083	0.6927
SD	0.0077	0.6563	SD	0.0077	0.6569
CP	84.0%	96.0%	CP	96.6%	95.9%

SE, mean of standard error estimates; SD, Monte Carlo standard deviation of the estimates across the simulated data; CP, coverage probability for the estimates.

and to test the difference between the diagnosis group in terms of the main effect and the shape effect.

Sample size were chosen as n = 200 participants with one eye per individual where 70% of the eyes does not have maculopathy and 30% of the eyes have maculopathy. In order to investigate how the spatial correlation can change the statistical inferences, we set three simulation scenarios in this section, one without correlation, one with a moderate ($\gamma_e = 0.5$) and the other with a high correlation ($\gamma_e = 0.1$) structure between different locations. All the simulation results in this section are based on 1000 Monte Carlo replications. The simulation results including the true parameter values, sample size, Monte Carlo standard deviation, the mean of standard error estimates, the coverage probabilities for the estimates and the power to detect the shape effect are reported in Tables 3, 4, 5 and 6.

In scenario 1 where no correlation exists between simulated outcomes, our spatial approach performed the same as the non-spatial approach in terms of the estimates when the sample size equals 200 (Table 3). The estimates were practically unbiased, the Monte Carlo standard deviation agreed with the mean of standard error estimates, and the coverage probability was around 95%, which is reasonable.

Table 5. Simulation studies: scenario 3: high exponential spatial correlation between simulated outcomes ($\gamma_e = 0.1$)

Non-spatial approach using linear regression			Spatial approach using linear mixed effect without correlation		
	Risk factor	Diagnosis for main effect		Risk factor	Diagnosis for main effect
True	−0.3	6.1	True	−0.3	6.1
n = 200	β_1	β_2	n = 200	β_1	β_2
Estimates	−0.3000	6.1180	Estimates	−0.3002	6.1120
SE	0.0056	0.6918	SE	0.0138	0.6927
SD	0.0170	0.7043	SD	0.0141	0.7033
CP	**57.2**%	95.1%	CP	94.9%	95.1%

SE, mean of standard error estimates; SD, Monte Carlo standard deviation of the estimates across the simulated data; CP, coverage probability for the estimates.

Table 6. Power of detecting the difference in shape between groups in spatial approach and non-spatial approach ($p < 0.01$)

Detection of shape effect $p < 0.01$	Non-spatial approach using linear regression	Spatial approach using linear mixed effect
No correlation	100%	100%
Moderate correlation	88.1%	95.3%
High correlation	88.9%	100%

For comparison, Tables 4 and 5 present the results based on moderate exponential correlation where $\gamma_e = 0.5$, and a high exponential correlation where $\gamma_e = 0.1$. In Table 4, we can see a lower coverage probability in the non-spatial approach compared with our spatial approach. When higher spatial correlations exist, the coverage probability for the estimates of β_1 is much worse (Table 5). Using our spatial approach, the estimates of the parameters were practically unbiased with a reasonable coverage probability both in a moderate correlation setting and a high correlation setting. As expected, when there is no correlation between the simulated data as reported in Table 6, the spatial approach and the non-spatial approach were the same in detecting the shape effect (i.e. the interaction term). However, our spatial approach performed much better in the other two correlation settings.

5 Discussion

Rather than analysing only the retinal thickness in central subfield (a Welch's test with winsorized variances was performed for retinal thickness between groups in central subfield, $p = 0.38 > 0.05$), we proposed here a nested linear mixed effect model to analyse spatially related data, generated from a study of DMO. We showed that this approach is capable of incorporating spatial correlations in images and the correlation between two eyes from the same patient, and we found differences in mean retinal thickness between no-maculopathy versus maculopathy group. We also showed an exponential spatial correlation between sectors provides the best model. Simulations demonstrated that our spatial approach is able to provide more accurate inference on the risk factor and has the ability to detect the main effect and shape effect between diagnostic groups. A further interesting study would be early detection of diabetic retinopathy to discriminate between healthy eyes from eyes with retinopathy but without DMO, which would be useful for clinicians in planning early treatment for patients.

Our approach can be applied to further investigate the spatial context of other features [8] in images with other retinal diseases such as diabetic retinopathy and central vascular occlusion with the aim of developing a flexible anistropic spatial dependency structures which can be adapted to other medical images. Moreover, it would be useful to predict the disease occurrence and the time of occurrence by extending our spatial modelling into spatio-temporal modelling which incorporates longitudinal images [14].

6 Conclusion

Spatially collected data from retinal images presents both important opportunities and challenges for understanding, detecting and diagnosing eye disease. We extend the standard analytic approach into spatial methods that adjust for spatial correlations between the image sectors and correlation between eyes from the same patients. Our simulation results confirmed the advantage of the spatial modelling to provide more powerful statistical inference: power increases from

88.1% to 95.3%, 88.9% to 100% for moderate or high spatial correlations. In the future, the spatial approach has the ability to extend the model into prediction or prognosis (i.e. the predictive modelling) and develop personal clinical management and monitoring tool.

Acknowledgement. Wenyue Zhu would like to acknowledge the PhD funding from Institute of Ageing and Chronic Disease and Institute of Translational Medicine at University of Liverpool and the Royal Liverpool University Hospital.

References

1. Bernal-Rusiel, J.L., et al.: Spatiotemporal linear mixed effects modeling for the mass-univariate analysis of longitudinal neuroimage data. Neuroimage **81**, 358–370 (2013)
2. Bowman, F.D., Waller, L.A.: Modelling of cardiac imaging data with spatial correlation. Stat. Med. **23**(6), 965–985 (2004)
3. BuAbbud, J.C., Al-latayfeh, M.M., Sun, J.K.: Optical coherence tomography imaging for diabetic retinopathy and macular edema. Curr. Diab. Rep. **10**(4), 264–269 (2010)
4. Cressie, N.: Statistics for spatial data. Terra Nova **4**(5), 613–617 (1992)
5. Laird, N.M., Ware, J.H., et al.: Random-effects models for longitudinal data. Biometrics **38**(4), 963–974 (1982)
6. Lindquist, M.A., et al.: The statistical analysis of fMRI data. Stat. Sci. **23**(4), 439–464 (2008)
7. MacCormick, I.J., et al.: Accurate, fast, data efficient and interpretable glaucoma diagnosis with automated spatial analysis of the whole cup to disc profile. PloS one **14**(1), e0209409 (2019)
8. MacCormick, I.J., et al.: Spatial statistical modelling of capillary non-perfusion in the retina. Sci. Rep. **7**(1), 16792 (2017)
9. Nussenblatt, R.B., Kaufman, S.C., Palestine, A.G., Davis, M.D., Ferris, F.L.: Macular thickening and visual acuity: measurement in patients with cystoid macular edema. Ophthalmology **94**(9), 1134–1139 (1987)
10. Pinheiro, J., Bates, D., DebRoy, S., Sarkar, D., R Core Team: nlme: Linear and Nonlinear Mixed Effects Models (2018). https://CRAN.R-project.org/package=nlme. R package version 3.1-137
11. Early Treatment Diabetic Retinopathy Study Research Group: Grading diabetic retinopathy from stereoscopic color fundus photographs-an extension of the modified Airlie House classification: ETDRS report no. 10. Ophthalmology **98**(5), 786–806 (1991)
12. Hee, M.R., et al.: Quantitative assessment of macular edema with optical coherence tomography. Arch. Ophthalmol. **113**(8), 1019–1029 (1995)
13. Van Buuren, S., Groothuis-Oudshoorn, K.: MICE: multivariate imputation by chained equations in R. J. Stat. Softw. **45**(3), 1–67 (2011). https://www.jstatsoft.org/v45/i03/
14. Vogl, W.D., Waldstein, S.M., Gerendas, B.S., Schmidt-Erfurth, U., Langs, G.: Predicting macular edema recurrence from spatio-temporal signatures in optical coherence tomography images. IEEE Trans. Med. Imaging **36**(9), 1773–1783 (2017)
15. Ying, G.S., Maguire, M.G., Glynn, R., Rosner, B.: Tutorial on biostatistics: linear regression analysis of continuous correlated eye data. Ophthalmic Epidemiol. **24**(2), 130–140 (2017)

16. Ying, G.S., Maguire, M.G., Glynn, R., Rosner, B.: Tutorial on biostatistics: statistical analysis for correlated binary eye data. Ophthalmic Epidemiol. **25**(1), 1–12 (2018)
17. Zhang, H.G., Ying, G.S.: Statistical approaches in published ophthalmic clinical science papers: a comparison to statistical practice two decades ago. Br. J. Ophthalmol. **102**(9), 1188–1191 (2018)